Environmental Science & Technology

pubs.acs.org/est

Article

Precise Cation Separations with Composite Cation-Exchange Membranes: Role of Base Layer Properties

Ryan M. DuChanois, Lauren Mazurowski, Hanqing Fan, Rafael Verduzco, Oded Nir, and Menachem Elimelech*

Cite This: *Environ. Sci. Technol.* 2023, 57, 6331−6341

Read Online

ACCESS | Metrics & More | Article Recommendations | Supporting Information

ABSTRACT: Separation of specific ions from water could enable recovery and reuse of essential metals and nutrients, but established membrane technologies lack the high-precision selectivity needed to facilitate a circular resource economy. In this work, we investigate whether the cation/cation selectivity of a composite cation-exchange membrane (CEM), or a thin polymer selective layer on top of a CEM, may be limited by the mass transfer resistance of the underlying CEM. In our analysis, we utilize a layer-by-layer technique to modify CEMs with a thin polymer selective layer (∼50 nm) that has previously shown high selectivity toward copper over similarly sized metals. While these composite membranes have a $CuCl_2/MgCl_2$ selectivity up to 33 times larger than unmodified CEMs in diffusion dialysis, our estimates suggest that eliminating resistance from the underlying CEM could further increase selectivity twofold. In contrast, the CEM base layer has a smaller effect on the selectivity of these composite membranes in electrodialysis, although these effects could become more pronounced for ultrathin or highly conductive selective layers. Our results highlight that base layer resistance prevents selectivity factors from being comparable across diffusion dialysis and electrodialysis, and CEMs with low resistance are necessary for providing highly precise separations with composite CEMs.

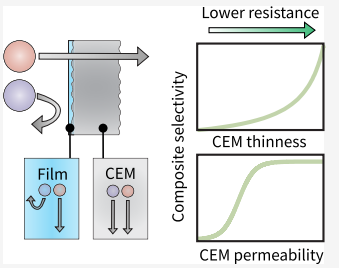

KEYWORDS: *polyelectrolyte multilayers, resource recovery, ion separations, electrodialysis, diffusion dialysis, Donnan dialysis*

INTRODUCTION

Water is an indispensable resource, not only for the water itself but also the valuable resources it contains. Many naturally occurring brines and wastewaters hold elements that are critical for producing modern technologies (e.g., copper, lithium, and cobalt) or crop fertilizers (e.g., phosphorus and ammonia).[1,2] Sustainable extraction of these critical elements could augment supplies of these minerals or offset carbon emissions associated with their traditional mining or production.[3] Of the separation approaches that are currently available for extracting such valuable metals and nutrients from water, electrodialysis (ED) is particularly attractive owing to its operational simplicity, energy efficiency, and low chemical requirements.[4−7]

ED is a process that uses an electric field to transport ions from a diluate solution through ion-exchange membranes (IEMs, or self-supported membranes with ionized functional groups) and into a concentrate solution.[8,9] Conventionally, IEMs are charge-dense, allowing only transport of species with opposite charge of the membrane (counterions) while excluding species with the same charge as the membrane (co-ions).[4] More specifically, negatively charged membranes that permit passage of cations are termed cation-exchange membranes (CEMs), while positively charged membranes that permit passage of anions are termed anion-exchange membranes (AEMs). The selective transport of counterions is one of the most desired properties of CEMs and AEMs because it is inextricably linked with the efficiency of ED as a process.[10]

While IEMs exhibit excellent permselectivity toward counterions, they are less effective in separating between counterions, especially when those counterions have similar physicochemical properties. Engineering membranes that separate like-charged species is a key prerequisite for extracting specific minerals from complex wastewaters and brines using ED.[11−13] Moderate selectivity between counterions is typically obtained by applying a thin selective layer to the IEM surface to form a composite structure.[14] For example, monovalent-selective IEMs are commercially available composites that pass monovalent ions and retain multivalent ions based on size, charge, or hydrophobicity.[15,16] Composite IEMs for separating counterions with similar physicochemical properties also exist, although they are in earlier stages of research and development.[17−19] For these more precise separations, the chemistry of the selective layer provides tailored interactions between target species and a membrane to enable preferential passage of that species.[20−23]

Received: January 18, 2023
Revised: March 29, 2023
Accepted: March 29, 2023
Published: April 6, 2023

https://doi.org/10.1021/acs.est.3c00445
Environ. Sci. Technol. 2023, 57, 6331−6341

While the addition of a thin selective layer can increase performance, the selectivity of the composite membrane is not necessarily that of the free-standing selective layer.[5] In gas separation membranes, the support layer resistance can pose performance-limiting effects, which are mitigated by a highly permeable intermediate layer (referred to as a gutter layer).[24] In thin-film composite membranes, which are the state-of-the-art technology for pressure-driven reverse osmosis, the porous structural support layer is often assumed to pose negligible resistance compared to the selective layer.[25] This assumption could break down, however, as the selective layer becomes more permeable or thinner, or as the support layer becomes less porous.[26,27] In principle, the pore structure of the support layer could affect the water/salt selectivity in reverse osmosis membranes under these circumstances.[26]

With the development of composite IEMs, there is question if the resistance of the IEM or "base layer" may limit the performance of the composite membrane, analogous to previous investigations on composite membranes in gas separations and reverse osmosis desalination. IEMs are polymer networks with substantial fixed charge concentrations that provide Donnan exclusion of co-ions.[15] These fixed charges may contribute considerable resistance to the composite membrane in a diffusion-driven process.[28,29] In an electro-driven process, these fixed charges provide high ionic conductivity (or low electrical resistance), but it is unclear whether this conductivity is adequate to render the IEM resistance negligible. Substantial resistance from IEMs could limit the selectivity of composite membranes, especially for ultrathin or low-resistance selective layers which are desirable for high-precision separations.[22]

In this study, we assess the effect of the ion permeability and conductivity of a CEM base layer on cation/cation selectivity of a composite CEM. For our analysis, we use polyelectrolyte layer-by-layer assembly to deposit a thin selective layer with demonstrated copper selectivity on a commercial CEM.[30] We then characterize the separation performance of the composite CEM in diffusion dialysis, Donnan dialysis, and ED, where the polymer selective layer markedly increased the Cu^{2+}/Mg^{2+} selectivity of the membrane and produced high-purity copper solutions in the presence of magnesium. Using systematic experiments and transport modeling, we subsequently estimate if the resistance of the CEM base layer limits the selectivity of the composite membrane. Our findings demonstrate that the separation performance of ultrathin or highly conductive polymer selective layers could be limited by base layer resistance, which highlights a practical consideration for maximizing selectivity of composite CEMs under some conditions.

MATERIALS AND METHODS

Materials and Chemicals. Poly(allylamine hydrochloride) (PAH, M_w 120−200 kDa) and anhydrous magnesium chloride ($MgCl_2$, 99%) were purchased from Alfa Aesar. Chloroacetic acid, copper(II) chloride ($CuCl_2$, 99%), sodium nitrate ($NaNO_3$, <99%), and potassium chloride (KCl, 99%) were purchased from Sigma-Aldrich. Sodium chloride (NaCl, 99%), nitric acid (HNO_3, 69.0−70.0%), sodium hydroxide (NaOH, >98%), and hydrochloric acid (HCl, 36.5−38%) were purchased from J.T. Baker. Compressed N_2 gas (ultrahigh purity) was purchased from Airgas. Ag/AgCl electrodes with porous Teflon tips (CHI111) and platinum wire electrodes (CHI115) were purchased from CH Instruments. Glass frits (G300) with 0.5−1 μm pore size were purchased from Princeton Applied Research.[31] Fumasep FKS-50 and FAD-55 (Fumatech) were purchased from Fuel Cell Store. Anodic aluminum oxide (AAO) membranes with a 25 mm diameter and 20 to 30 nm pore diameter were obtained from Hefei Pu-Yuan Nanotechnology Ltd. N-type silicon wafers with 300 nm wet thermal oxide were purchased from UniversityWafer, Inc. Deionized (DI) water (18 MΩ-cm) used throughout synthesis and experimentation was obtained from a Milli-Q system with Elix Technology (EMD Millipore). All reagents and materials were used as received unless otherwise specified.

Cation-Exchange Membrane Characterization. The commercial CEMs used in this study, Fumasep FKS, are homogeneous membranes without any fabric backing for mechanical support. The CEMs, also referred to as "pristine" membranes, were provided in H^+ form. Relevant properties of these membranes, including water uptake, ion-exchange capacity, and thickness, are available in product specification sheets by the manufacturer, which are presented in Table S1. Prior to use, the CEMs were cut into smaller coupons (~5 cm^2) and placed in 0.5 M NaCl solution (200 mL) for at least 24 h to put the membrane in Na^+ form and remove any additives or preservatives from the membrane, unless otherwise specified.

Hydrated thicknesses of pristine CEMs (δ_p) were measured using a digital micrometer (Mitotuyo Series 293−340). After soaking membrane coupons in aqueous solution of one or more salts ($CuCl_2$, $MgCl_2$) for at least 24 h, five thickness measurements were made over the area of the membrane and averaged. Membranes were returned to the solution between each measurement to ensure full hydration. No changes in membrane thickness were detectable for the concentrations of the solutions used in this study (Table S2).

Membrane Surface Modification. Poly[*N*,*N*-dicarboxymethyl allylamine] (PDCMAA) was synthesized as described previously.[22,32] Polymer deposition solutions were prepared with 10 mM polyelectrolyte (PAH or PDCMAA) and 0.5 M NaCl. The properties of these polymers are available in Table S3. We note that polymer concentrations are calculated with respect to the repeating unit, and PDCMAA concentrations are likely overestimated because of adsorbed NaCl and water to the PDCMAA. Polymer solutions were adjusted to pH 3.0 using dilute HCl to protonate PAH ($pK_a \approx 9.3$) and partially protonate carboxylate groups of PDCMAA ($pK_a \approx 1.8$, 2.6).[33,34]

Polyelectrolyte multilayer films were formed on non-reinforced, homogeneous CEMs via layer-by-layer assembly to form a composite membrane, unless otherwise noted. The CEM was placed between two rubber gaskets, which were clamped together between a glass plate and a hollow polytetrafluoroethylene (PTFE) frame using stainless-steel binder clips. Polycation solution (10 mM PAH) was pipetted into the hollow PTFE frame to immerse one side of the CEM for 5 min. During this time, the membrane was set on a shake plate (60 rpm). After removing the PAH solution, the membrane was continuously rinsed with DI water for 1 min to remove any loosely adsorbed PAH. Subsequently, polyanion solution (PDCMAA) was pipetted into the hollow PTFE frame and left for 5 min while shaking (60 rpm). The membrane was then rinsed with DI water for 1 min, which completed the assembly of one polyelectrolyte bilayer. This process was repeated to produce $(PAH/PDCMAA)_n$ films of n bilayers (n = 3−7). Finally, membranes were rinsed and stored

https://doi.org/10.1021/acs.est.3c00445
Environ. Sci. Technol. 2023, 57, 6331−6341

in DI water until use. Similar methods were used to form these films on positively charged AAO substrates, except that $(PDCMAA/PAH)_{3.5}$ films were deposited onto the substrate. For AAO substrates, PDCMAA was the first layer, contrary to FKS membranes.

Multilayer Film Characterization. A Dektak XT stylus profilometer (Bruker) was used to investigate polyelectrolyte film thickness (δ_f).[22] Polyelectrolyte multilayers were assembled with identical methods as described for CEMs, with the exception that silicon wafers were utilized as substrates. Prior to layer-by-layer assembly, silicon wafers were cleaned for 10 min with an ultraviolet/ozone cleaner (BioForce Nanosciences ProCleaner Plus), thoroughly rinsed with DI water, dried with N_2 gas, and dried for 24 h in ambient air. Polyelectrolyte films were then carefully sliced with a metal precision glide needle (18G × 1 in) without damaging the underlying wafer. Subsequently, the following profilometer settings were implemented: a tip radius of 12.5 μm, stylus scan range of 65.5 μm (z-resolution ≈ 1 nm), stylus force of 5 mg, and scanning time of 15 s. Single step-height measurements were calculated by averaging the thickness over a large bandwidth (>50 μm) perpendicular to the direction of the slice. Reported step heights are the averages of measurements collected at three randomly selected positions along the needle slice. Measurements are representative of the dry thickness of the polyelectrolyte film, which are likely smaller than the wet (or swollen) thickness.

We performed attenuated total reflectance Fourier-transform infrared spectroscopy (ATR−FTIR) and static water contact angle measurements to verify the deposition of $(PDCMAA/PAH)_5$ films on CEMs. Prior to measurements, samples were dried for 24 h in a vacuum. ATR−FTIR measurements were collected using a Shimadzu IRTracer-10 with 20 scans at 2 cm^{-1} resolution. The static contact angle of the membranes was measured by a contact angle goniometer (OneAttension, Biolin) using the sessile drop method. Within 30 min of removing the membrane from vacuum, a 5-μL droplet was placed on the membrane surface and the water droplet was imaged using a digital camera. Images were processed using OneAttension software.

Diffusion and Donnan Dialysis. Concentration-driven diffusion testing was conducted with a custom-made, glass diffusion cell with two 60 mL chambers and a temperature-controlled water jacket. A membrane (1.77 cm^2) was mounted between the two chambers with the modified side toward the feed chamber, unless otherwise specified. The feed chamber contained one salt ($CuCl_2$ or $MgCl_2$) in single-salt experiments and two salts ($CuCl_2$ and $MgCl_2$) in multisalt experiments. Feed solutions were adjusted to pH 3.6 using 1.0 M HCl to prevent metal hydrolysis, while the receiving chambers contained DI water unless otherwise specified. Each chamber was continuously mixed using magnetic stir bars and stir plates. We assume concentration polarization to be negligible in this system because of the rapid stirring. The water jacket temperature was maintained at 25 ± 0.1 °C with a cooling/heating circulator (Cole Parmer Polystat) to control the internal temperature of the feed and receiving chambers.

During testing, 0.5 mL samples were initially taken from the feed and receiving chambers (t = 0) and then every 30 min to 1 h after approaching the steady state. Sampling both chambers ensured each chamber contained approximately the same volume throughout the experiment. Water transport induced by osmotic pressure difference prevented exactly equal volumes in each compartment from being retained but was determined to be negligible, unless otherwise specified. Initial samples from the feed chamber (t = 0) were diluted 10,000 times, and all samples from the receiving chamber were diluted 10 times with 1% (v/v) HNO_3. These samples were analyzed using inductively coupled plasma mass spectroscopy (ICP−MS, ELAN DRC-e, Perkin Elmer) to quantify divalent cation concentrations.

The concentration change in the receiving compartment over the testing period was negligible compared to the feed concentration (<0.5%), which ensured a near-constant driving force during experiments. After an initial time, the moles of salt in the receiving chamber began to linearly increase with time, which allowed calculation of a flux according to

$$J_i = \frac{V_r}{A_m}\left(\frac{dC_{r,i}}{dt}\right) \tag{1}$$

where J_i is the flux of solute i, V_r is the volume in the receiving chamber, A_m is the effective membrane area (1.77 cm^2), and $\frac{dC_{r,i}}{dt}$ is the concentration change of solute i in the receiving chamber with respect to time. Notably, in diffusion dialysis, coupling effects occur between one cation and one anion, such that they permeate at the same rate (as a salt) to maintain electroneutrality on each side of the membrane.

If we assume concentration polarization to be negligible because of continuous stirring in the feed and receiving chambers, steady-state permeability (P_i) and permeance (B_i) of solute i can be calculated according to

$$B_i = \frac{P_i}{\delta} = \frac{J_i}{C_{f,i}} \tag{2}$$

where δ is the effective membrane thickness and $C_{f,i}$ is the concentration of solute i in the feed chamber. It is also important to note that the inverse of the permeance of solute i is resistance (R_i). Membrane selectivity can then be expressed as

$$S = \frac{J_i/C_{f,i}}{J_j/C_{f,j}} = \frac{P_i}{P_j} \tag{3}$$

where S is the selectivity for solute i over solute j, J_j is the flux of solute j, $C_{f,j}$ is the concentration of solute j in the feed chamber, and P_j is the permeability of solute j. Error bars were determined with standard propagation of uncertainty methods and represent one standard deviation (SD) from three fabricated membranes.

Electrodialysis. ED experiments were conducted in batch mode with a four-compartment glass cell (schematic illustration in the Results and Discussion). A single cell pair configuration was used with an effective membrane area of 2.0 cm^2. The cathode and anode chambers (~75 mL) were separated from the diluate and concentrate chambers using a commercial AEM (Fumasep FAD). The diluate and concentrate chambers (~10 mL) were separated by either a pristine or modified FKS CEM, where the modified surface faced the diluate chamber (toward the anode). The stack consisted of three IEMs in total, including two AEMs and one CEM. Membranes were stored in a 0.5 M NaCl solution when not in use.

The electrode chambers contained 0.4 M $NaNO_3$ solution and were constantly mixed using a peristaltic pump (Masterflex

https://doi.org/10.1021/acs.est.3c00445
Environ. Sci. Technol. 2023, 57, 6331−6341

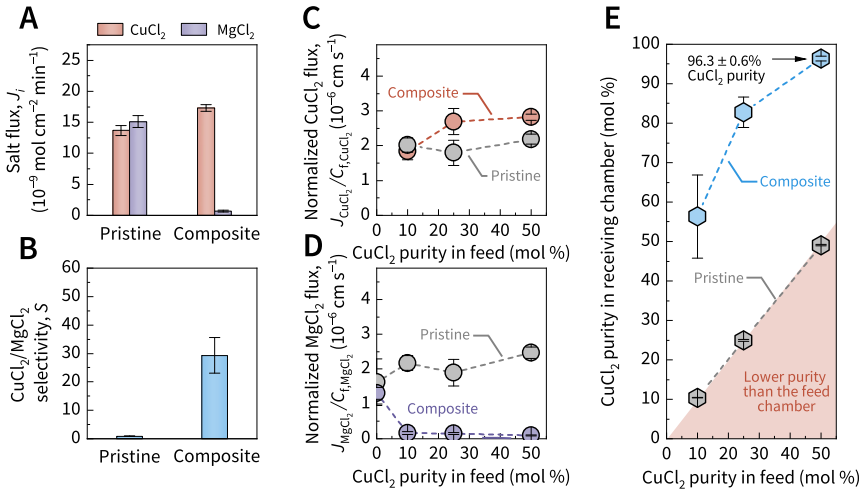

Figure 1. Copper selectivity of composite CEMs with polyelectrolyte multilayer films as selective layers. (A) Salt flux and (B) $CuCl_2/MgCl_2$ selectivity in multisalt feed solutions of 0.1 M $CuCl_2$ and 0.1 M $MgCl_2$ (pH 3.6). FKS membranes were modified on the side facing the feed chamber with $(PAH/PDCMAA)_5$ films. (C) Normalized $CuCl_2$ flux, (D) normalized $MgCl_2$ flux, and (E) $CuCl_2$ purity in the receiving chamber for pristine and composite membranes with multisalt feed solutions containing $CuCl_2$ and $MgCl_2$ concentrations of different molar proportions (or $CuCl_2$ purity). In (C) and (D), fluxes were normalized to the molar feed concentration in the feed chamber of their respective salt ($C_{f,i}$ for solute i). In (E), the red region represents selectivity that yields lower copper purity in the receiving chamber than the feed chamber. Experiments were conducted with a total ionic strength of 0.6 M (pH 3.6) as the feed solution (comprising $CuCl_2$ and $MgCl_2$). All experiments were conducted with DI water as the receiving solution. All error bars represent one SD of three independent measurements.

L/S, Cole-Parmer) at a flow rate of 5 mL min^{-1} to counterbalance pH changes from electrode reactions. Electrode reservoirs were adjusted to pH 2 with HNO_3 prior to testing, and the pH of the electrode reservoirs was monitored for the duration of testing and adjusted as necessary with HNO_3 or NaOH. The diluate reservoir contained 0.1 M $CuCl_2$ and 0.1 M $MgCl_2$, and the concentrate reservoir contained 10 mM HCl. Diluate and concentrate reservoirs were adjusted to pH 2 with HCl prior to testing. Each chamber was continuously mixed using magnetic stir bars.

A voltage was applied to generate a constant current (2 mA, 1.0 mA cm^{-2}) using an Agilent E3617A power supply. Next, 50 μL aliquots were taken from the diluate and concentrate reservoirs every 10−20 min for 2−4 h. All samples were diluted 100 times with 1% (v/v) HNO_3 and analyzed using ICP−MS. Solute fluxes were calculated using eq 2, which were then converted to transport numbers using[35]

$$t_i = \frac{J_i z_i F}{I} \tag{4}$$

where t_i is the transport number of solute i in the membrane, z_i is the valence of solute i, F is the Faraday constant, and I is the current density. Eq 4 assumes that ion transport is dominated by migration from the electric field over diffusive and advective transport.[36] Subsequently, the membrane selectivity for solute i over solute j was calculated as[36]

$$S = \frac{z_j}{z_i}\frac{t_i/C_{f,i}}{t_j/C_{f,j}} = \frac{J_i/C_{f,i}}{J_f/C_{f,j}} \tag{5}$$

where t_j is the transport number of solute j in the membrane and z_j is the valence of solute j. Error bars were determined with standard propagation of uncertainty methods and represent one SD from three fabricated membranes.

Membrane Conductivity. Membrane conductivity measurements were performed using a four-electrode electrochemical setup.[13] Membranes were equilibrated in the testing solution (0.1 M $CuCl_2$ or $MgCl_2$) for 24 h prior to measurement. The membrane (2.0 cm^2) was then mounted between two ∼75 mL glass chambers, which were identical to the electrode chambers from ED experiments. Both chambers contained the same solutions of 0.1 M $CuCl_2$ or 0.1 M $MgCl_2$ and were adjusted to pH 3.6 using dilute HCl. It should be noted that the divalent cation concentration was large compared to the proton concentration (≈0.25%). Both chambers were well-mixed using magnetic stir bars and stir plates.

Platinum wire electrodes and Ag/AgCl reference electrodes (1 M KCl, CH Instruments) were placed in each chamber. The Ag/AgCl reference electrodes were sealed in custom-made Haber−Luggin capillaries (2 mm inner diameter, filled with 1 M KCl). The tip of the capillaries held borosilicate glass frits (Princeton Applied Research), which were attached to the capillaries with Teflon heat shrink tubing. The capillaries were then mounted into each chamber of the glass cell and stationed less than 5 mm from the membrane.[37]

Current was passed between the platinum wire electrodes using a Keithley 2400 Series SourceMeter. We then measured the potential difference across the membrane using the Ag/AgCl reference electrodes for nine steps between current densities of 0.025−0.25 mA cm^{-2}. Each current density was maintained for 30 s prior to recording the potential difference across the membrane. The background potential drop, or the potential drop measured without the membrane present between the glass cell, was also measured. The area specific electrical resistance (r_i) and the resistivity (ρ_i) of the membrane toward solute i were then determined from the slope of the total potential drop as a function of current density $\left(\frac{dV_t}{dI}\right)$, minus the resistance attributable to the solution $\left(\frac{dV_s}{dI}\right)$:[38]

$$r_i = \rho_i \delta = \frac{dV_t}{dI} - \frac{dV_s}{dI} \tag{6}$$

The inverse of the resistance and resistivity toward solute i are the area specific conductance (G_i) and conductivity (κ_i),

https://doi.org/10.1021/acs.est.3c00445
Environ. Sci. Technol. 2023, 57, 6331−6341

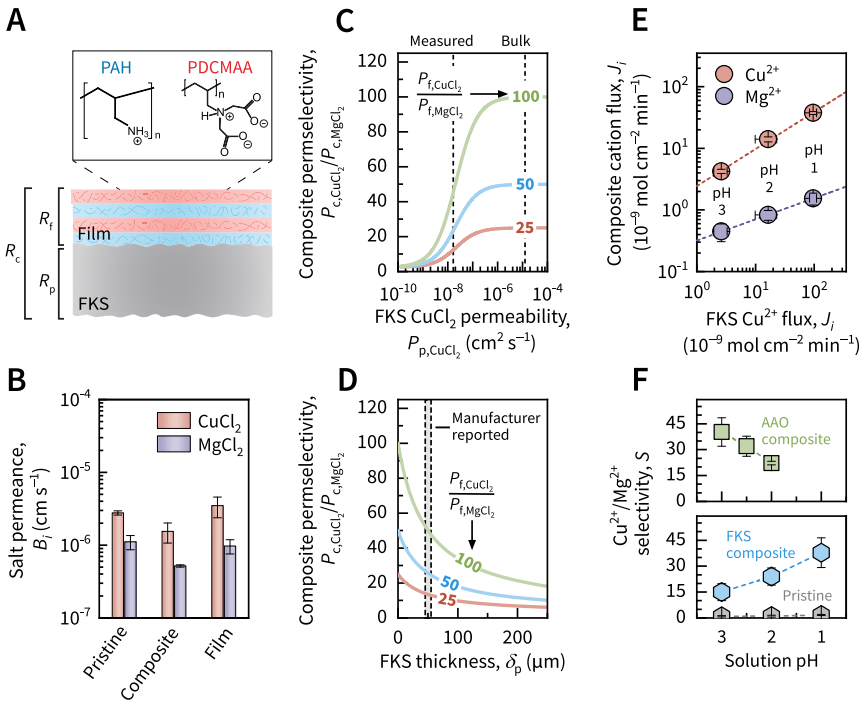

Figure 2. Effect of the CEM base layer on the selectivity of the composite membrane in diffusion and Donnan dialysis. (A) Schematic illustration of the resistance-in-series method for determining the salt permeance of the polyelectrolyte film. The salt resistance of the composite membrane (R_c) was assumed to be equal to the sum of the salt resistances of the pristine FKS membrane (R_p) and polyelectrolyte film (R_f). Composite FKS membranes have five bilayers of (PAH/PDCMAA)$_5$ films (only two bilayers are shown). Not drawn to scale. (B) Salt permeance for pristine FKS membranes, composite FKS membranes with (PAH/PDCMAA)$_5$ films, and only (PAH/PDCMAA)$_5$ films. Experiments were conducted with 0.1 M $CuCl_2$ or $MgCl_2$ (pH 3.6) as the single-salt feed solution and DI water as the receiving solution. (C, D) Modeled $CuCl_2/MgCl_2$ permselectivity of a composite membrane with changing the (C) salt permeability and (D) thickness of the pristine membrane with a film permselectivity ($P_{f,\,CuCl_2}/P_{f,\,MgCl_2}$) assumed to be 25, 50, or 100. Salt permeability and permselectivity of the pristine membrane were determined from (B). The modeled composite permselectivity was derived from eq 8. In (C), the vertical dashed lines indicate the measured $CuCl_2$ permeability of the pristine membrane and the diffusivity of $CuCl_2$ in bulk water.[41] In (D), the gray dashed line indicates the thickness of the pristine FKS membrane reported by the manufacturer (Table S1). (E, F) Effect of increasing the cation flux of the unmodified CEM on (E) the cation flux of the composite membrane and (F) Cu^{2+}/Mg^{2+} selectivity of pristine and composite membranes. The flux of the pristine membrane was increased by lowering the pH of the feed and receiving solutions (pH 1–3) using HCl. FKS composite membranes had (PAH/PDCMAA)$_5$ films (δ_f = 51 nm), and AAO composites had (PDCMAA/PAH)$_{3.5}$ films (δ_f = 35 nm, ref 22). Experiments were conducted with equimolar $CuCl_2$ and $MgCl_2$ (0.1 M) in a multisalt feed solution. All error bars represent one SD of three independent measurements.

respectively. Error bars were determined with standard propagation of uncertainty methods and represent one SD from three fabricated membranes.

RESULTS AND DISCUSSION

Ultrathin Selective Layer Increases Composite Selectivity. Pristine CEMs are unable to discriminate between cations of similar size and charge effectively.[4,39,40] To increase the selectivity of CEMs for a specific cation, we applied n bilayers of PAH and PDCMAA (n = 3–7) on the surface of Fumasep CEMs, which we denote as (PAH/PDCMAA)$_n$. We confirmed the surface modification of the CEMs using ATR–FTIR spectroscopy. Peaks at 1630 and 3350 cm^{-1} are characteristic of N–H stretching and $-COO^-$ asymmetric stretching and consistent with the composition of (PAH/PDCMAA)$_n$ coatings (Figure S1). Static water contact angle measurements provide additional evidence of surface modification, as the hydrophilicity of the CEMs increased appreciably with addition of (PAH/PDCMAA)$_5$ films (Figure S2). From here forward, we refer to the (PAH/PDCMAA)$_n$ coating as a "film" and the pristine CEM+ the (PAH/PDCMAA)$_n$ film as a "composite".

We tested transport of $CuCl_2$ and $MgCl_2$ salts through these membranes in a temperature-controlled diffusion cell, where a salt concentration difference across the membrane provided a driving force between the concentrated feed chamber and dilute receiving chamber of DI water. After an initial time-lag when salt transport across the membrane had not yet reached the steady state, metal concentrations in the receiving chamber were measured over time using ICP–MS, from which we calculated salt flux. The $CuCl_2$ and $MgCl_2$ fluxes through the pristine FKS membrane were similar when these species were simultaneously present in equimolar concentrations in the feed compartment, which was expected given their similar diffusion coefficients in bulk water (1.26 and 1.25 × 10^{-5} cm^2 s^{-1}, respectively) (Figure 1A).[41] The $CuCl_2/MgCl_2$ selectivity associated with these flux values is 0.89 ± 0.08 (Figure 1B).

In contrast, after applying a 51-nm (PAH/PDCMAA)$_5$ film to these CEMs (Figure S3), the $CuCl_2/MgCl_2$ selectivity markedly increased to 29.0 ± 4.25 (Figure 1B). Similar selectivity was also observed when both sides of the FKS membrane were modified with (PAH/PDCMAA)$_5$ films (Figure S4 and Text S1). This enhancement in selectivity compared to the pristine CEM can be primarily attributed to the low $MgCl_2$ flux through the polyelectrolyte film, as

https://doi.org/10.1021/acs.est.3c00445
Environ. Sci. Technol. 2023, 57, 6331–6341

discussed in prior work with these films on alumina supports.[30] In brief, copper outcompetes magnesium for iminodiacetate chelating groups within the polyelectrolyte film (Table S3), which reduces magnesium sorption in proportion with its binding energy to iminodiacetate groups.[22] More details about the mechanism for membrane selectivity are available in the Supporting Information (Text S2).

While these composite membranes exhibit exceptional selectivity, it is notable that concentration-normalized $CuCl_2$ fluxes are relatively similar to those of the pristine membrane for a range of feed solution conditions (Figures 1C and S5, Text S3 and S4). The normalized $MgCl_2$ fluxes of the pristine and composite membranes were also comparable before copper was introduced and considerably hindered magnesium passage (see the 0% $CuCl_2$ purity condition in Figure 1D). This behavior suggests that the polymer selective layer may pose little additional resistance to salt transport compared to the CEM base layer. In this case, the relatively high resistance of the CEM base layer toward mass transfer could lower the selectivity factors obtained with the composite membrane. More explicitly, the composite membrane, even though it can considerably upgrade the $CuCl_2$ purity of dilute solutions (Figures 1E and S6), may have lower selectivity than the polymer selective layer. In the following section, we investigate whether the selectivity of the composite CEM may be limited by the low salt permeability (or high salt resistance) of the CEM base layer when using a concentration difference as the driving force for salt transport.

CEM Resistance Limits Composite Selectivity in Diffusion Dialysis. CEMs with a thin selective layer of iminodiacetate groups provide high selectivity for copper, but it is unclear whether the underlying CEM affects the separation performance of the composite. To investigate this possibility, we determined salt permeances through pristine and composite membranes in diffusion dialysis, where we used solutions of 0.1 M $CuCl_2$ or $MgCl_2$ (single salts) in the feed chamber and DI water in the receiving chamber. We then used a resistance-in-series approach to estimate salt permeance through the polyelectrolyte film:[42−45]

$$\frac{1}{B_{f,i}} = \frac{1}{B_{c,i}} - \frac{1}{B_{p,i}} \tag{7}$$

where $B_{f,i}$, $B_{c,i}$, and $B_{p,i}$ are the permeances of solute i (cm s^{-1}) through the polyelectrolyte film, composite membrane, and pristine CEM, respectively (Figure 2A). With this method, we determined the salt permeance of a standalone $(PAH/PDCMAA)_5$ film to be roughly the same order of magnitude as the salt permeance of the pristine membrane (Figure 2B), which can be attributed to the dense structure and/or strong cation−polymer interactions of the thin film.

Salt permeability values were subsequently used to determine the effect of the pristine CEM on the composite membrane permselectivity using the resistance-in-series model (Figure S7). The composite membrane permselectivity can be written as follows:

$$\frac{P_{c,i}}{P_{c,j}} = \frac{R_{f,j} + R_{p,j}}{R_{f,i} + R_{p,i}} \tag{8}$$

where $P_{c,i}/P_{c,j}$ is the composite membrane permselectivity for solute i and j, $R_{f,i}$ and $R_{f,j}$ are the resistances of solute i and j through the polyelectrolyte film, and $R_{p,i}$ and $R_{p,j}$ are the resistances of solute i and j through the pristine CEM (more details about the model and assumptions are available in the Supporting Information, Text S5 and S6). According to the model, the composite permselectivity approaches the permselectivity of the pristine membrane when the resistance of the pristine membrane is high. Conversely, the composite permselectivity approaches the permselectivity of the (PAH/PDCMAA) film when the resistance of the pristine membrane is low.

We modeled how changing the permeability and thickness of the pristine membrane affects the $CuCl_2/MgCl_2$ permselectivity of the composite membrane, all else equal (Figure 2C,D). More specifically, we arbitrarily assumed film permselectivity values (that is, $P_{f,CuCl_2}/P_{f,MgCl_2}$) of 25, 50, or 100 (see contour lines in Figure 2C,D). For each assumed film permselectivity, we then estimated the composite membrane permselectivity for any given permeability or thickness of the CEM base layer. It is important to note that this approach inherently assumes that the permselectivity of the CEM does not change across the range of CEM permeabilities and thicknesses considered (Text S6).

Experimental data were subsequently layered on top of the model to evaluate whether the properties of the CEM base layer limit the permselectivity of the composite membrane. The experimentally measured $CuCl_2$ permeability of the pristine membrane falls toward the left side of the plot in Figure 2C. In this region, the model estimates that the composite permselectivity is constrained to less than half of the assumed permselectivity of the film. The composite membrane permselectivity is no longer limited by the base layer, however, as the $CuCl_2$ permeability of the pristine membrane increases. For instance, the CEM base layer has a negligible effect on the composite membrane permselectivity as its $CuCl_2$ permeability approaches its theoretical maximum value, or the diffusivity of $CuCl_2$ in bulk water.

The thickness of the pristine membrane has a similar limiting effect on the permselectivity of the composite membrane as the permeability of the pristine membrane (Figure 2D). The CEM thickness, as reported by the manufacturer (45−55 μm), presents enough mass transfer resistance where the composite membrane permselectivity is considerably lower than the assumed permselectivity of the film. A much thinner CEM with otherwise similar properties could provide much higher $CuCl_2/MgCl_2$ permselectivity, according to the model.

We then experimentally investigated whether decreasing the CEM resistance would increase selectivity of the composite membrane. We performed Donnan dialysis using multisalt feed solutions of 0.1 M $CuCl_2$ and $MgCl_2$ with the pH of the feed and receiving chambers adjusted with HCl. Unlike diffusion dialysis, protons can diffuse from the receiving chamber to the feed chamber while metal cations diffuse from the feed chamber to the receiving chamber. Acid addition thus allows protons to "pump" metal cations across the CEM.[46] This process should yield higher fluxes because it is not rate-limited by the slow transport of anions (co-ions) across the CEM, as seen with diffusion dialysis. Rising Cu^{2+} and Mg^{2+} fluxes through the pristine membrane with more HCl confirm that protons pump Cu^{2+} and Mg^{2+} into the receiving chamber (Figure 2E).

If the resistance of the CEM limits the selectivity of the composite membrane, increasing transport rates through the CEM should increase the Cu^{2+} flux more than the Mg^{2+} flux for

https://doi.org/10.1021/acs.est.3c00445
Environ. Sci. Technol. 2023, 57, 6331−6341

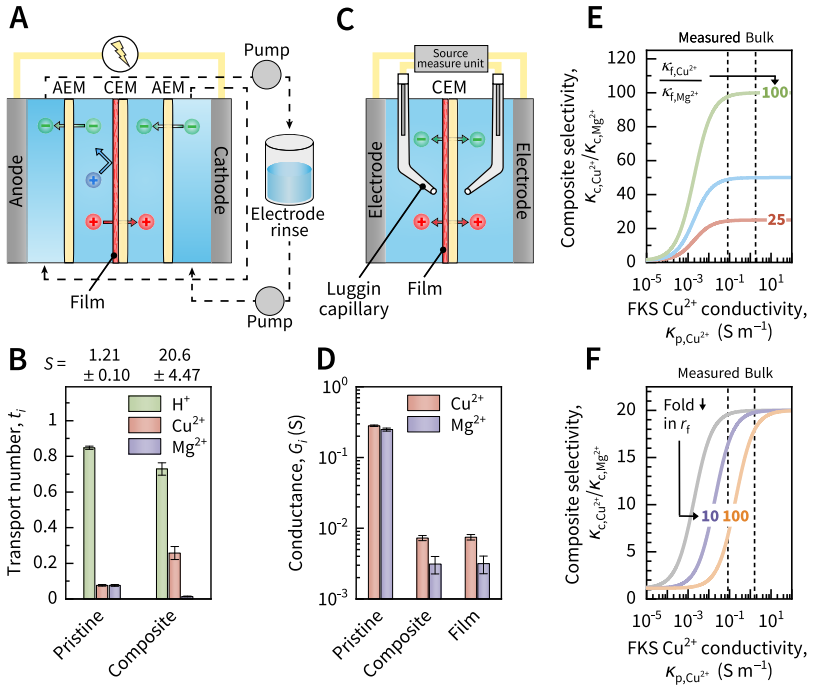

Figure 3. Effect of the CEM base layer on the selectivity of the composite membrane in ED. (A) Schematic illustration of the four-compartment ED system. The cathode and anode chambers were recirculated to an external electrode rinse solution using peristaltic pumps. A CEM separated the diluate chamber (facing the anode) and the concentrate chamber (facing the cathode). (B) Transport numbers of H^+, Cu^{2+}, and Mg^{2+} for pristine FKS membranes and composite FKS membranes with $(PAH/PDCMAA)_5$ films. The Cu^{2+}/Mg^{2+} selectivity (S) of each membrane is listed above the chart. Experiments were conducted with 0.1 M $CuCl_2$ and 0.1 M $MgCl_2$ (pH 2) in a multisalt diluate chamber, 10 mM HCl (pH 2) in the concentrate chamber, and 0.4 M $NaNO_3$ (pH 2) in the electrode chambers. A constant current density of 1 mA cm^{-2} (2 mA) was used. (C) Illustration of the two-compartment cell used to determine membrane resistance and conductance. Ag/AgCl reference electrodes were placed in Luggin capillaries filled with 1 M KCl and stationed within 5 mm of the membrane. (D) Conductance for pristine FKS membranes, composite FKS membranes with $(PAH/PDCMAA)_5$ films, and only $(PAH/PDCMAA)_5$ films. Films faced the anode. Experiments were conducted with single-salt solutions of 0.1 M $CuCl_2$ or $MgCl_2$ (pH 3.6) in both chambers. (E, F) Modeled Cu^{2+}/Mg^{2+} selectivity of a composite membrane with changing the conductivity of the pristine membrane with a (E) film selectivity ($\kappa_{f,Cu^{2+}}/\kappa_{f,Mg^{2+}}$) assumed to be 25, 50, or 100 or (F) film resistance (r_f) that is 10- or 100-fold lower than experimentally determined (gray curve). Conductivity and selectivity of the pristine membrane were determined from (D). The modeled composite selectivity was derived from eq 10. The vertical dashed lines indicate the measured Cu^{2+} conductivity of the pristine membrane and the conductivity of $CuCl_2$ in bulk water.[41] In (F), the film selectivity was assumed to be 20 in accordance with (B). All error bars represent one SD of three independent measurements.

the composite membrane. We observe this behavior when adding acid into the receiving chamber to increase fluxes through the CEM (Figure 2E). The Cu^{2+} flux increases considerably more than the Mg^{2+} flux of the composite membrane as the mass transfer resistance of the pristine membrane decreases. More explicitly, the slope of the trendline for Cu^{2+} is steeper than that for Mg^{2+} in Figure 2E, suggesting an increase in Cu^{2+}/Mg^{2+} selectivity of the composite membrane at lower pH.

Alternatively, an increase of selectivity at low pH could be explained if the Cu^{2+}/Mg^{2+} selectivity of the bare CEM or $(PDCMAA/PAH)_5$ film increased. As expected, the Cu^{2+}/Mg^{2+} selectivity of the pristine FKS membrane changed very little across pH 1−3 (Figure 2F, bottom), which removes the possibility that the pristine FKS membrane enhances composite membrane selectivity at low pH. We then investigated whether the film selectivity increased at lower pH by preparing polyelectrolyte films on AAO (δ_p = 61 μm) with 20−30 nm pore sizes and high porosity.[47] These large pore sizes minimize the resistance of the base layer, at least compared to CEMs, which in principle should reduce effects of the base layer on the selectivity of the composite membrane. The selectivity of a polyelectrolyte film on AAO is thus expected to approximate the selectivity of the polyelectrolyte film. We determined the separation performance of AAO composite membranes with solution acidity down to pH 2 (AAO was unstable at pH 1), and the film did not become more selective in more acidic environments (Figure 2F, top). Instead, the film became less selective at lower pH, perhaps because the film increasingly favored proton sorption over copper (Figure S8). Although different base layers may lend films with distinct properties and performance, it appears reasonable to conclude that the film did not contribute to the higher selectivity of the FKS composite membrane at low pH.

If an increase in selectivity of the bare CEM or film did not increase selectivity of the FKS composite membrane at low pH, we can attribute the increase in selectivity to the lower resistance of the CEM base layer (Figure 2F, bottom). More specifically, a lower resistance of the pristine CEM allows the composite membrane selectivity to approach the selectivity of the film. This analysis supports that the resistance of the CEM base layer restricts the selectivity of the composite membrane in diffusion experiments. Increasing the salt permeance of the CEM base layer could improve composite membrane selectivity, but other driving forces for ion transport may also reduce the mass transfer resistance of the CEM base layer. In the following section, we measure the ionic conductivity of the

https://doi.org/10.1021/acs.est.3c00445
Environ. Sci. Technol. 2023, 57, 6331−6341

CEM to determine if it may limit the Cu^{2+}/Mg^{2+} selectivity of a composite material in ED.

Lowering CEM Resistance Maximizes Composite Selectivity. A four-compartment ED system was used to evaluate pristine and modified CEMs for their Cu^{2+}/Mg^{2+} selectivity at a constant current density of 1 mA cm^{-2} (Figure 3A). The applied voltage provided similar fluxes through the pristine membrane and 4−7 times higher fluxes through the composite membrane than observed in Donnan dialysis under identical conditions (Figures 2E and S9). These fluxes suggest that the Donnan potential in Donnan dialysis and the applied potential in ED are approximately equal for the pristine membrane.

Protons were the dominant charge carriers for both pristine and composite membranes (Figure 3B), which is reasonable given the mobility of protons and the solution acidity (pH 2). For the pristine membrane, Cu^{2+} and Mg^{2+} carried small but nearly equal fractions of the current (~0.08) (Figure 3B). In contrast, the Cu^{2+} transport number increased to 0.26 ± 0.04 and the Mg^{2+} transport number decreased to 0.01 ± 0.002 with addition of the $(PAH/PDCMAA)_5$ film. These transport numbers correspond to Cu^{2+}/Mg^{2+} selectivity of 1.21 ± 0.10 for the pristine membrane and 20.6 ± 4.47 for the composite membrane. Notably, the composite membrane selectivity in ED is comparable to the selectivity observed in Donnan dialysis under identical conditions (24.0 ± 4.93, Figure 2F).

To establish whether the CEM base layer affects the composite membrane selectivity, we used a four-electrode, two-compartment system equipped with Haber−Luggin capillaries to determine the ionic conductivity of the pristine and modified membranes (Figure 3C). Lower conductances were observed for composite membranes with $(PAH/PDCMAA)_5$ films facing the anode than the cathode (Figure S10 and Text S7). To maintain consistency with the experimental design in ED testing, we calculated the conductance of a polyelectrolyte thin film facing the anode using a resistance-in-series approach:[42−45]

$$\frac{1}{G_{f,i}} = \frac{1}{G_{c,i}} - \frac{1}{G_{p,i}} \tag{9}$$

where $G_{f,i}$, $G_{c,i}$, and $G_{p,i}$ are the conductances of solute i (S) through the polyelectrolyte film, composite membrane, and pristine CEM, respectively (Figure S11). The conductance of the standalone $(PAH/PDCMAA)_5$ film was 1−2 orders of magnitude smaller than the conductance of the pristine membrane (Figure 3D), which is a considerably larger difference than observed for permeances (Figure 2B).

Ionic conductivities of each component of the composite membrane were then used to model composite membrane selectivity as follows:

$$\frac{\kappa_{c,i}}{\kappa_{c,j}} = \frac{r_{f,j} + r_{p,j}}{r_{f,i} + r_{p,i}} \tag{10}$$

where $\kappa_{c,i}/\kappa_{c,j}$ is the composite membrane selectivity for solutes i and j, $r_{f,i}$ and $r_{f,j}$ are the electrical resistances of solutes i and j through the polyelectrolyte film, and $r_{p,i}$ and $r_{p,j}$ are the electrical resistances of solutes i and j through the pristine CEM (more details about the model and assumptions are available in Text S6 and S8). Specifically, we evaluated whether the conductivity of the pristine CEM bears any effect on the Cu^{2+}/Mg^{2+} selectivity of the composite membrane, assuming that conductivity of the base layer may be tuned independently from other properties (Figure 3E). Similar to methods described in the prior section, we assumed film selectivities (in this case, $\kappa_{f,Cu^{2+}}/\kappa_{f,Mg^{2+}}$) of 25, 50, or 100 (see contour lines in Figure 3E) to model the composite membrane selectivity for a range of CEM conductivities.

Conductivity measurements from experiments were then layered onto the model to assess whether the composite membrane selectivity is partially controlled by the CEM base layer (Figure 3E). According to our estimates, the conductivity of the CEM base layer, as measured in experiments, has a negligible effect on the composite membrane selectivity for any assumed film selectivity. Increasing the conductivity of the CEM base layer, even to the conductivity of the bulk solution, would not provide noticeable improvement in the selectivity of the composite material.

Nonetheless, the effect of the base layer could become more pronounced as the electrical resistance of the base layer increases or the polyelectrolyte film decreases. For example, in Figure 3F, we use the resistance-in-series model to estimate how a 10- or 100-fold lower film resistance (contour lines in Figure 3F) could change the composite membrane selectivity as a function of CEM conductivity. At the conductivity measured for FKS membranes, a 100-fold decrease in the electrical resistance of the film could reduce the composite selectivity by more than twofold, according to model estimates. As there can be considerable variability in the conductivity and thickness of selective layers, it seems possible that some films may have 10 to 100 times lower resistance than the $(PAH/PDCMAA)_5$ films studied here. Future ED studies should consider on a case-by-case basis whether a CEM base layer could have performance-limiting effects on a composite membrane.

IMPLICATIONS

Membranes with highly precise selectivity between similar species could enable various separations of considerable water, energy, and environmental significance, such as nutrient recycling from wastewater, water softening, and reclamation of critical metals from brines or wastewaters.[3,6,13,48] Applying a thin selective layer on an IEM is a common method used to produce selectivity between similar ions, including commercial monovalent-selective membranes and lab-scale membranes with ion-specific selectivity.[15−19] With this method, the mass transfer resistance of the IEM base layer is typically assumed to bear no effect on the selectivity of the composite membrane. Our work demonstrates otherwise—the resistance of the IEM can be performance-limiting under some circumstances.

Understanding the conditions in which the mass transfer resistance of the base layer influences composite membrane performance is critical to proper design and experimental evaluation of these materials. Results from this study highlight that resistance of IEMs can vary with the driving force for ion transport, indicating that IEMs have a distinct effect on composite membrane selectivity in different processes. Separation factors measured across these different driving forces are therefore not necessarily similar. Membranes developed for specific purposes should be evaluated with the methods in which they were designed to be used,[6] but we recommend to avoid testing composite IEMs in diffusion dialysis. In this process, Donnan exclusion of co-ions produces high resistance to salt transport that can considerably affect the separation performance of the composite.

https://doi.org/10.1021/acs.est.3c00445
Environ. Sci. Technol. 2023, 57, 6331−6341

While we did not observe any performance-limiting effects of the base layer on the composite membrane selectivity in ED, conclusions may change for composite IEMs with base layers that have considerably lower conductivity and larger thickness than FKS. As an example, AEMs generally have lower conductivity than CEMs,[49] such that thick AEM base layers could have more pronounced effects on the composite membrane selectivity. It is also possible that other separations which involve monovalent or trivalent counterions could lend different outcomes. Given that the potential influence of the IEM resistance on composite membrane selectivity is now apparent, future studies with other base layers, selective layers, and salt pairs should consider these effects. These studies will provide a more complete understanding of whether IEM base layers influence composite membrane selectivity in ED.

Designing composite IEMs with precise selectivity may require that attention be given to engineering novel IEMs as base layers. The mass transfer resistance of the base layer could become less negligible as the selective layers become more permeable or thinner,[5] which are otherwise desirable goals for high-precision ion separations.[22] Designing IEMs with higher conductivity or lower thickness should thus be considered, although the effect of these design choices on other performance metrics should be carefully evaluated. For instance, ionic conductivity can be improved by increasing ion-exchange capacity (that is, the number of ion-exchange groups per unit weight of dry polymer), but the cation/anion permselectivity would decrease because of swelling of the membrane.[50] Reducing membrane thickness would also reduce resistance, but it may compromise mechanical stability.[51] Novel materials or fabrication methods that decrease mass transfer resistance of IEMs without forfeiting other key properties will be necessary for practical, high-precision membrane separations.

■ ASSOCIATED CONTENT

Supporting Information

The Supporting Information is available free of charge at https://pubs.acs.org/doi/10.1021/acs.est.3c00445.

Salt resistance and selectivity of double-sided composite membranes (Text S1); mechanism for membrane selectivity (Text S2); transport behavior and mechanisms with varying feed purity (Text S3); transport behavior and mechanisms with varying feed ionic strength (Text S4); resistance-in-series model for permeability (Text S5); model assumptions (Text S6); conductance with the film facing the anode or anode (Text S7); resistance-in-series model for conductivity (Text S8); attenuated total reflectance Fourier-transform infrared spectra of composite CEMs (Figure S1); static water contact angles for pristine and composite CEMs (Figure S2); thickness of layer-by-layer polyelectrolyte films with 4−7 bilayers (Figure S3); transport properties of composite CEMs with single-sided or double-sided modification (Figure S4); normalized salt flux and selectivity for pristine and composite membranes in diffusion dialysis with multisalt feed solutions of different ionic strength (Figure S5); selectivity in diffusion dialysis with multisalt feed solutions of different molar proportions (Figure S6); $CuCl_2/MgCl_2$ permselectivity of pristine CEMs, modified CEMs, and polyelectrolyte films in diffusion dialysis with single-salt solutions (Figure S7); cation flux of AAO composite membranes at different pH (Figure S8); fluxes of Cu^{2+} and Mg^{2+} in ED (Figure S9); conductance of $(PAH/PDCMAA)_5$ films facing the anode or cathode (Figure S10); Cu^{2+}/Mg^{2+} selectivity of pristine CEMs, modified CEMs, and polyelectrolyte films calculated from conductivity measurements (Figure S11); properties of cation-exchange membranes reported by the manufacturer (Table S1); experimentally determined thickness of cation-exchange membranes (Table S2); and properties of polymers utilized in layer-by-layer assembly (Table S3) (PDF)

■ AUTHOR INFORMATION

Corresponding Author

Menachem Elimelech − *Department of Chemical and Environmental Engineering, Yale University, New Haven, Connecticut 06520-8286, United States; Nanosystems Engineering Research Center for Nanotechnology-Enabled Water Treatment (NEWT), Houston, Texas 77005, United States;* orcid.org/0000-0003-4186-1563; Phone: +1 (203) 432 2789; Email: menachem.elimelech@yale.edu

Authors

Ryan M. DuChanois − *Department of Chemical and Environmental Engineering, Yale University, New Haven, Connecticut 06520-8286, United States; Nanosystems Engineering Research Center for Nanotechnology-Enabled Water Treatment (NEWT), Houston, Texas 77005, United States;* orcid.org/0000-0002-3463-5958

Lauren Mazurowski − *Department of Chemical and Environmental Engineering, Yale University, New Haven, Connecticut 06520-8286, United States; Nanosystems Engineering Research Center for Nanotechnology-Enabled Water Treatment (NEWT), Houston, Texas 77005, United States*

Hanqing Fan − *Department of Chemical and Environmental Engineering, Yale University, New Haven, Connecticut 06520-8286, United States*

Rafael Verduzco − *Nanosystems Engineering Research Center for Nanotechnology-Enabled Water Treatment (NEWT), Houston, Texas 77005, United States; Department of Chemical and Biomolecular Engineering, Materials Science and NanoEngineering, Rice University, Houston, Texas 77005, United States;* orcid.org/0000-0002-3649-3455

Oded Nir − *Department of Desalination and Water Treatment, Zuckerberg Institute for Water Research, The Jacob Blaustein Institutes for Desert Research, Ben-Gurion University of the Negev, Midreshet Ben Gurion 8499000, Israel;* orcid.org/0000-0003-2061-9188

Complete contact information is available at: https://pubs.acs.org/10.1021/acs.est.3c00445

Notes

The authors declare no competing financial interest.

■ ACKNOWLEDGMENTS

This work was financially supported by the US National Science Foundation (NSF) and US−Israel Binational Science Foundation (BSF) under award no. CBET-2110138 and the Engineering Research Center for Nanotechnology-Enabled Water Treatment under award no. EEC-1449500. We also

acknowledge the Abel Wolman Fellowship from the American Water Works Association awarded to R.M.D. and the NSF Graduate Research Fellowship awarded to L.M. Facilities used for profilometry were supported by the Yale Institute of Nanoscale and Quantum Engineering (YINQE). We also thank J. Karosas for assistance with ICP−MS at Yale Analytical and Stable Isotope Center (YASIC). Yale Glass Shop provided the diffusion cell, electrodialysis cell, and Luggin capillaries.

REFERENCES

(1) Epsztein, R.; DuChanois, R. M.; Ritt, C. L.; Noy, A.; Elimelech, M. Towards Single-Species Selectivity of Membranes with Subnanometre Pores. *Nat. Nanotechnol.* **2020**, *15*, 426−436.
(2) Li, Y.; Wang, R.; Shi, S.; Cao, H.; Yip, N. Y.; Lin, S. Bipolar Membrane Electrodialysis for Ammonia Recovery from Synthetic Urine: Experiments, Modeling, and Performance Analysis. *Environ. Sci. Technol.* **2021**, *55*, 14886−14896.
(3) DuChanois, R. M.; Cooper, N. J.; Lee, B.; Patel, S. K.; Mazurowski, L.; Graedel, T. E.; Elimelech, M. Prospects of Metal Recovery from Wastewater and Brine. *Nat. Water* **2023**, *1*, 37−46.
(4) Geise, G. M.; Paul, D. R.; Freeman, B. D. Fundamental Water and Salt Transport Properties of Polymeric Materials. *Prog. Polym. Sci.* **2014**, *39*, 1−42.
(5) Park, H. B.; Kamcev, J.; Robeson, L. M.; Elimelech, M.; Freeman, B. D. Maximizing the Right Stuff: The Trade-off between Membrane Permeability and Selectivity. *Science* **2017**, *356*, 1137.
(6) Wang, R.; Zhang, J.; Tang, C. Y.; Lin, S. Understanding Selectivity in Solute−Solute Separation: Definitions, Measurements, and Comparability. *Environ. Sci. Technol.* **2022**, *56*, 2605−2616.
(7) Patel, S. K.; Qin, M.; Walker, W. S.; Elimelech, M. Energy Efficiency of Electro-Driven Brackish Water Desalination: Electrodialysis Significantly Outperforms Membrane Capacitive Deionization. *Environ. Sci. Technol.* **2020**, *54*, 3663−3677.
(8) Luo, T.; Abdu, S.; Wessling, M. Selectivity of Ion Exchange Membranes: A Review. *J. Membr. Sci.* **2018**, *555*, 429−454.
(9) Strathmann, H. Electrodialysis, a Mature Technology with a Multitude of New Applications. *Desalination* **2010**, *264*, 268−288.
(10) Ji, Y.; Luo, H.; Geise, M. Specific Co-Ion Sorption and Diffusion Properties Influence Membrane Permselectivity. *J. Membr. Sci.* **2018**, *563*, 492−504.
(11) Sujanani, R.; Landsman, M. R.; Jiao, S.; Moon, J. D.; Shell, M. S.; Lawler, D. F.; Katz, L. E.; Freeman, B. D. Designing Solute-Tailored Selectivity in Membranes: Perspectives for Water Reuse and Resource Recovery. *ACS Macro Lett.* **2020**, *9*, 1709−1717.
(12) Zuo, K.; Wang, K.; DuChanois, R. M.; Fang, Q.; Deemer, E. M.; Huang, X.; Xin, R.; Said, I. A.; He, Z.; Feng, Y.; Shane Walker, W.; Lou, J.; Elimelech, M.; Huang, X.; Li, Q. Selective Membranes in Water and Wastewater Treatment: Role of Advanced Materials. *Mater. Today* **2021**, *50*, 516−532.
(13) Fan, H.; Huang, Y.; Billinge, I. H.; Bannon, S. M.; Geise, G. M.; Yip, N. Y. Counterion Mobility in Ion-Exchange Membranes: Spatial Effect and Valency-Dependent Electrostatic Interaction. *ACS ES&T Engg.* **2022**, *2*, 1274−1286.
(14) Sata, T.; Yamaguchi, T.; Matsusaki, K. Preparation and Properties of Composite Membranes Composed of Cation-Exchange Membranes and Polypyrrole. *J. Phys. Chem.* **1996**, *100*, 16633−16640.
(15) DuChanois, R. M.; Porter, C. J.; Violet, C.; Verduzco, R.; Elimelech, M. Membrane Materials for Selective Ion Separations at the Water−Energy Nexus. *Adv. Mater.* **2021**, *33*, No. 2101312.
(16) Wormser, E. M.; Nir, O.; Edri, E. Low-Resistance Monovalent-Selective Cation Exchange Membranes Prepared Using Molecular Layer Deposition for Energy-Efficient Ion Separations. *RSC Adv.* **2021**, *11*, 2427−2436.
(17) Sata, T.; Tagami, Y.; Matsusaki, K. Transport Properties of Anion-Exchange Membranes Having a Hydrophobic Layer on Their Surface in Electrodialysis. *J. Phys. Chem. B* **1998**, *102*, 8473−8479.
(18) Ding, D.; Yaroshchuk, A.; Bruening, M. L. Electrodialysis through Nafion Membranes Coated with Polyelectrolyte Multilayers Yields >99% Pure Monovalent Ions at High Recoveries. *J. Membr. Sci.* **2022**, *647*, No. 120294.
(19) Yang, S.; Liu, Y.; Liao, J.; Liu, H.; Jiang, Y.; van der Bruggen, B.; Shen, J.; Gao, C. Codeposition Modification of Cation Exchange Membranes with Dopamine and Crown Ether to Achieve High K^+ Electrodialysis Selectivity. *ACS Appl. Mater. Interfaces* **2019**, *11*, 17730−17741.
(20) Warnock, S. J.; Sujanani, R.; Zofchak, E. S.; Zhao, S.; Dilenschneider, T. J.; Hanson, K. G.; Mukherjee, S.; Ganesan, V.; Freeman, B. D.; Abu-Omar, M. M.; Bates, C. M. Engineering Li/Na Selectivity in 12-Crown-4 Functionalized Polymer Membranes. *Proc. Natl. Acad. Sci. U. S. A.* **2021**, *118*, No. e2022197118.
(21) Lounder, S. J.; Asatekin, A. Interaction-Based Ion Selectivity Exhibited by Self-Assembled, Cross-Linked Zwitterionic Copolymer Membranes. *Proc. Natl. Acad. Sci. U. S. A.* **2021**, *118*, No. e2022198118.
(22) DuChanois, R. M.; Heiranian, M.; Yang, J.; Porter, C. J.; Li, Q.; Zhang, X.; Verduzco, R.; Elimelech, M. Designing Polymeric Membranes with Coordination Chemistry for High-Precision Ion Separations. *Sci. Adv.* **2022**, *8*, No. eabm9436.
(23) Zhou, X.; Heiranian, M.; Yang, M.; Epsztein, R.; Gong, K.; White, C. E.; Hu, S.; Kim, J.-H.; Elimelech, M. Selective Fluoride Transport in Subnanometer TiO_2 Pores. *ACS Nano* **2021**, *15*, 16828−16838.
(24) Kattula, M.; Ponnuru, K.; Zhu, L.; Jia, W.; Lin, H.; Furlani, E. P. Designing Ultrathin Film Composite Membranes: The Impact of a Gutter Layer. *Sci. Rep.* **2015**, *5*, 15016.
(25) Aghajani, M.; Wang, M.; Cox, L. M.; Killgore, J. P.; Greenberg, A. R.; Ding, Y. Influence of Support-Layer Deformation on the Intrinsic Resistance of Thin Film Composite Membranes. *J. Membr. Sci.* **2018**, *567*, 49−57.
(26) Ramon, G. Z.; Wong, M. C. Y.; Hoek, E. M. V. Transport through Composite Membrane, Part 1: Is There an Optimal Support Membrane? *J. Membr. Sci.* **2012**, *415*−*416*, 298−305.
(27) Davenport, D. M.; Ritt, C. L.; Verbeke, R.; Dickmann, M.; Egger, W.; Vankelecom, I. F. J.; Elimelech, M. Thin Film Composite Membrane Compaction in High-Pressure Reverse Osmosis. *J. Membr. Sci.* **2020**, *610*, No. 118268.
(28) Gokturk, P. A.; Sujanani, R.; Qian, J.; Wang, Y.; Katz, L. E.; Freeman, B. D.; Crumlin, E. J. The Donnan Potential Revealed. *Nat. Commun.* **2022**, *13*, 5880.
(29) Donnan, F. G. The Theory of Membrane Equilibria. *Chem. Rev.* **1924**, *1*, 73−90.
(30) Sheng, C.; Wijeratne, S.; Cheng, C.; Baker, G. L.; Bruening, M. L. Facilitated Ion Transport through Polyelectrolyte Multilayer Films Containing Metal-Binding Ligands. *J. Membr. Sci.* **2014**, *459*, 169−176.
(31) Mousavi, M. P. S.; Saba, S. A.; Anderson, E. L.; Hillmyer, M. A.; Bühlmann, P. Avoiding Errors in Electrochemical Measurements: Effect of Frit Material on the Performance of Reference Electrodes with Porous Frit Junctions. *Anal. Chem.* **2016**, *88*, 8706−8713.
(32) Naka, K.; Tachiyama, Y.; Hagihara, K.; Tanaka, Y.; Yoshimoto, M.; Ohki, A.; Maeda, S. Synthesis and Chelating Properties of Poly[*N*,*N*-Dicarboxymethyl)Allylamine] Derived from Poly-(Allylamine). *Polym. Bull.* **1995**, *35*, 659−663.
(33) Shiratori, S. S.; Rubner, M. F. pH-Dependent Thickness Behavior of Sequentially Adsorbed Layers of Weak Polyelectrolytes. *Macromolecules* **2000**, *33*, 4213−4219.
(34) Martell, A. E.; Smith, R. M. *Critical Stability Constants*; Springer: New York, 1990; Vol. *6*.
(35) Sata, T. *Ion Exchange Membranes: Preparation, Characterization, Modification and Application*; Royal Society of Chemistry, 2007.
(36) Luo, H.; Agata, W. A. S.; Geise, G. M. Connecting the Ion Separation Factor to the Sorption and Diffusion Selectivity of Ion Exchange Membranes. *Ind. Eng. Chem. Res.* **2020**, *59*, 14189−14206.
(37) Galama, A. H.; Hoog, N. A.; Yntema, D. R. Method for Determining Ion Exchange Membrane Resistance for Electrodialysis Systems. *Desalination* **2016**, *380*, 1−11.

https://doi.org/10.1021/acs.est.3c00445
Environ. Sci. Technol. 2023, 57, 6331−6341

(38) Fan, H.; Huang, Y.; Yip, N. Y. Advancing the Conductivity-Permselectivity Tradeoff of Electrodialysis Ion-Exchange Membranes with Sulfonated CNT Nanocomposites. *J. Membr. Sci.* **2020**, *610*, No. 118259.
(39) Kamcev, J.; Paul, D. R.; Manning, G. S.; Freeman, B. D. Predicting Salt Permeability Coefficients in Highly Swollen, Highly Charged Ion Exchange Membranes. *ACS Appl. Mater. Interfaces* **2017**, *9*, 4044−4056.
(40) Epsztein, R.; Shaulsky, E.; Qin, M.; Elimelech, M. Activation Behavior for Ion Permeation in Ion-Exchange Membranes: Role of Ion Dehydration in Selective Transport. *J. Membr. Sci.* **2019**, *580*, 316−326.
(41) Vanýsek, P. Ionic Conductivity and Diffusion at Infinite Dilution. In *CRC Handbook of Chemistry and Physics*, 1996; pp 77−79.
(42) Henis, J. M. S.; Tripodi, M. K. Composite Hollow Fiber Membranes for Gas Separation: The Resistance Model Approach. *J. Membr. Sci.* **1981**, *8*, 233−246.
(43) Crank, J. *The Mathematics of Diffusion*, 2nd ed.; Oxford University Press: New York, 1979.
(44) Werber, J. R.; Porter, C. J.; Elimelech, M. A Path to Ultraselectivity: Support Layer Properties to Maximize Performance of Biomimetic Desalination Membranes. *Environ. Sci. Technol.* **2018**, *52*, 10737−10747.
(45) Cheng, C.; Yaroshchuk, A.; Bruening, M. L. Fundamentals of Selective Ion Transport through Multilayer Polyelectrolyte Membranes. *Langmuir* **2013**, *29*, 1885−1892.
(46) Winston, W. S.; Sirkar, K. K. *Membrane Handbook*; Springer Science+Business Media, 1992; Vol. *1*.
(47) Wang, Y.; Lee, J.; Werber, J. R.; Elimelech, M. Capillary-Driven Desalination in a Synthetic Mangrove. *Sci. Adv.* **2020**, *6*, No. eaax5253.
(48) Tang, C.; Bruening, M. L. Ion Separations with Membranes. *J. Polym. Sci.* **2020**, *58*, 2831−2856.
(49) Kamcev, J. Reformulating the Permselectivity-Conductivity Tradeoff Relation in Ion-Exchange Membranes. *J. Polym. Sci.* **2021**, *59*, 2510−2520.
(50) Geise, G. M.; Hickner, M. A.; Logan, B. E. Ionic Resistance and Permselectivity Tradeoffs in Anion Exchange Membranes. *ACS Appl. Mater. Interfaces* **2013**, *5*, 10294−10301.
(51) Fan, H.; Yip, N. Y. Elucidating Conductivity-Permselectivity Tradeoffs in Electrodialysis and Reverse Electrodialysis by Structure-Property Analysis of Ion-Exchange Membranes. *J. Membr. Sci.* **2019**, *573*, 668−681.

https://doi.org/10.1021/acs.est.3c00445
Environ. Sci. Technol. 2023, 57, 6331−6341